Digest Journal of Nanomaterials and Biostructures Vol. 18, No. 4, October-December 2023, p.1275-1292

Study on the properties of 8YSZ thermal barrier coatings by atmospheric plasma spraying

J. J. Li[a], Y. F. Zhang[a,*], Q. Li[b], Q. Hao[c], X.Y. Ran[c], X. L. Guo[a]
[a]*School of Mechanical Engineering, Qilu University of Technology (Shandong Academy of Sciences), Jinan, Shandong, 250353, PR China*
[b]*School of Material Science and Engineering, Qilu University of Technology (Shandong Academy of Sciences), Jinan, Shandong, 250353, PR China*
[c]*Weihai Yinxing Prestressed Wire Products Co.,Ltd, Weihai, Shandong, 264200, PR China*

The 8 wt.% yttrium oxide partially stabilized zirconia (8YSZ) coatings were prepared by atmospheric plasma spraying (APS). The microstructure and properties of the coating were analyzed. The results show that the overall morphology of 8YSZ coating is smooth. The XRD pattern shows that the 8YSZ coating don't undergo phase transformation and has a stable tetragonal phase. 8YSZ thermal barrier coating (TBC) remains intact after 70 thermal cycle tests. The finite element results show that the 8YSZ TBC has good thermal insulation. Potentiodynamic polarization and electrochemical impedance spectroscopy show that the coating has good corrosion resistance.

(Received July 1, 2023; Accepted October 21, 2023)

Keywords: Atmospheric plasma spraying, 8YSZ, Thermal shock resistance, Corrosion resistance

1. Introduction

Thermal barrier coatings (TBCs) are a layer of ceramic coatings used to protect substrate materials, and TBCs play an important role in protecting superalloys from oxidation, erosion, wear, high temperature and large heat flow directly affecting the surface of superalloy substrates. It has been widely used on the hot-section components. The structure of TBCs mainly includes a substrate, a metal bond coating, a thermally grown oxide (TGO) and a ceramic top coating[1-3]. During the service of hot section components, the temperature of the metal coating often reaches a level that leads to the oxidation of the intermediate coating and the inevitable generation of TGO between the top and bond coatings[4, 5]. Because of its excellent high temperature resistance, low thermal conductivity and good corrosion resistance, ceramic materials are usually used as the top coating, which isolates the alloy matrix from high-temperature gas and reduces its temperature. The function of the metal bond coating is to compensate for the mismatch between the thermal expansion coefficient of the ceramic top coating and the alloy substrate, to improve the

* Corresponding author: zhangyanfei@qlu.edu.cn
https://doi.org/10.15251/DJNB.2023.184.1275

compatibility between the ceramic top coating and the alloy substrate, to relieve the internal stress of the coating, and to enhance the oxidation resistance of the coating[6]. The most widely used and successful ceramic top coating in TBCs materials is still 8YSZ material[7-9]. It has the characteristics of excellent thermal insulation performance, high durability, low thermal conductivity, high thermal expansion coefficient, and high melting point. However, its use is limited to temperatures below 1473 K, because the failure caused by high-temperature sintering and phase transformation makes it difficult for the coating to serve at higher temperatures[10]. Three methods are commonly used to prepare TBCs, namely atmospheric plasma spraying (APS)[11-13], electron beam-physical vapor deposition (EB-PVD)[14], and plasma spraying-physical vapor deposition (PS-PVD)[15]. Pores and microcracks are usually randomly distributed in the interior of TBCs[16-18]. The TBCs can protect the substrate and improve the service temperature and related service performance of the substrate[19, 20]. Therefore, it is of great significance to study TBCs.

In this paper, 8YSZ coatings were prepared using atmospheric plasma spraying technology, and the properties of 8YSZ coatings such as microscopic morphology, Vickers hardness, bond strength, surface roughness, thermal cycling test and corrosion resistance were investigated.

2. Experiment Procedures

2.1. Coating Deposition

Commercially available 8YSZ powder (-125+11 μm, 8 wt. % Y_2O_3-ZrO_2, Oerlikon Metco) was used as the ceramic top coating material. NiCoCrAlYTa (-38+5 μm, Amdry 997, Oerlikon Metco) was used as the bond coating material, which serves to limit the oxidation of the substrate, reduce the coefficient of thermal expansion (CTE) mismatch, and increase the adhesion of the ceramic top coating to the substrate[21, 22]. Improve the bonding strength between the coating and the substrate, preventing the coating from breaking and falling off during cooling. The sample substrate is aluminum alloy (ZL109), and its composition is shown in Table 1. Before spraying, use 60-mesh white corundum for sandblasting treatment, and the compressed air pressure is 0.6-0.8 MPa. The purpose of sandblasting is to remove surface impurities and increase the roughness of the coating surface. The atmospheric plasma spraying equipment uses the ZB-80K spraying system of Beijing Aerospace Zhenbang Precision Machinery Co., Ltd. and the spraying gas is a combination of argon and hydrogen. The spraying parameters of bonding coating and ceramic surface top coating are shown in Table 2. The structure of TBC is shown in Fig. 1. The ceramic top coating is usually thicker than the bond coating, which resists large heat flows directly affecting the substrate[23, 24]. The entire spraying process is performed indoors to prevent excessive oxidation from occurring while the coating is forming. After spraying, the samples were air-cooled to room temperature to prevent large internal stresses between the coatings. Samples were collected and further analysis was performed on the samples.

Table 1. Chemical composition of aluminum alloy ZL109 (wt.%).

Si	Cu	Mg	Ni	Fe	Zn	Ti	Sn	Pb	Al
11-13	0.5-1.5	0.8-1.3	0.8-1.5	0-0.7	≤0.2	≤0.2	≤0.01	≤0.05	Bal.

Table 2. Plasma spraying process parameters.

Power	NiCoCrAlYTa	8YSZ
Voltage (V)	61	69
Current (A)	585	633
Primary gas flow (L/min)	30	30
Secondary gas flow (L/min)	3	3
Power feed rate (RPM)	5	5
Spray distance (mm)	120	135

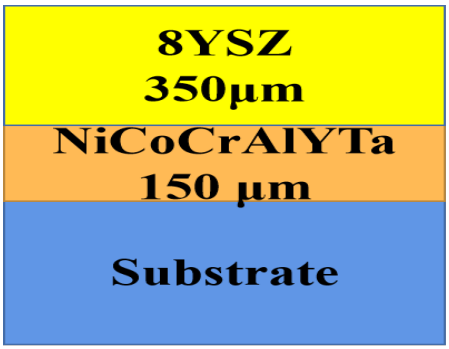

Fig. 1. Structural diagram of TBC.

2.2. Material Characterization

The X-ray diffraction analysis (SmartlabSE, Rigaku, Japan) was used for phase detection, the target was Cu target, the working voltage was 40 kV, the working current was 100 mA, the scanning range was 10-80°, and the scanning speed was 20°/min. Scanning electron microscopy (GeminiSEM 500, Carl Zeiss, Germany) was used to observe the surface and cross-section of the sprayed powder and coating to analyze their morphology and microstructure, and energy dispersive spectroscopy was used to analyze the composition of the coating surface and cross-section, as well as the elemental distribution. The thermogravimetric differential thermal analyzer (NETZSCH, Germany) was used to observe the thermal stability of the samples. The samples were heated in a nitrogen-protected alumina crucible with the following experimental parameters: temperature rise rate of 0.5 ℃/s from room temperatureto 1500 ℃.

Micro Vickers hardness tester (HXD-1000TMC) was used to measure the Vickers hardness of the coating with a test load of 2.942 N and a loading time of 20 s. The measurement of microhardness is carried out on the cross-section of the coating after grinding and polishing, and the measurement takes 6 points to take the average value. The laser spectral confocal microscope (KC-XI000, KathMatic) was used to measure surface roughness of coatings.

The samples were aligned and bonded to the axis of the tensile test bar using high permeability epoxy resin and slowly tightened with a wrench. The sample was then placed in a muffle furnace (SXL-1200C) for 60 min and heated to 100 ℃ and held for 180 min. After that, the sample bar was removed and the excess resin was removed from the surface, and the bonding strength of the coatings was measured by putting the sample bar into the universal testing machine (WDW-300E) for tensile testing. Each batch of at least 3 groups of paired parts, measure 3 valid data and take the average value.

The piston was put into the muffle furnace (SXL-1200C) and heated to 550 ℃ and kept warm for 20 min. After reaching the specified time, the piston was removed and put into room temperature water for rapid cooling, and the cooling time was 2 min. Then used a hair dryer to dry the surface moisture, observe whether the coating surface falls off and measure the weight, which is one cycle; multiple cycle experiments were carried out. The three-dimensional finite element model of the 8YSZ thermal barrier coating was established using ANSYS software and simulated for steady-state thermal analysis.

The coating and substrate were tested for corrosion in 3.5 wt% NaCl solution using an electrochemical workstation (CHI660E) at room temperature. A three-electrode system was used in the experiment: 8YSZ coating and substrate with an exposed area of 1 cm^2 were used as working electrodes, a saturated calomel electrode was used as a reference electrode, and a platinum sheet was used as an auxiliary electrode. First, in order to obtain the steady-state potential, an open circuit potential (OCP) test was performed for 3600 s. Electrochemical impedance spectroscopy (EIS) was then performed between 0.01 Hz and 100 kHz. Subsequently, the dynamic potential polarization curves were measured for the potential variation range −1–0.8 V (vs OCP) at a scan rate of 0.5 mV/s.

3. Results and Discussion

3.1. Powder Characteristics

The chemical composition of NiCoCrAlYTa powder is shown in Table 3. The microscopic morphology of NiCoCrAlYTa powder is shown in Fig. 2. The powder is prepared by a gas atomization process, and the principle of atomization powder making method is to use a high-pressure gas as an atomization medium to break up a continuous fine stream of molten metal, which forms a metal or alloy powder after subsequent cooling and solidification[25]. Among them, the powder prepared by this process shows regular spherical shape, smooth surface and good flowability. The particle size distribution of NiCoCrAlYTa powder is shown in Fig. 3. It has been shown that MCrAlY (M=Ni, Co or NiCo, etc.) has good oxidation resistance, ductility, high strength and thermal corrosion resistance[26-29]. Ni has the ability to relieve thermal stress, while Co has excellent oxidation resistance and thermal corrosion resistance. On the premise of ensuring corrosion resistance, Cr can also promote Al to form Al_2O_3 to improve oxidation resistance, but

high concentration of Al will damage the coating strength. Therefore, the concentration of Al should be reduced as much as possible while meeting the antioxidant requirements[30, 31]. The addition of Y to the powder promotes the chemical bonding between the oxide layer and the substrate, improving the cyclic oxidation performance of the coating system[32]. Chen et al[33] found that the addition of Ta element improved the oxidation resistance of the coating. The slowly formed dense Al_2O_3 film and the microstructure of the coating (as shown in Fig. 7) inhibited element diffusion and contributed to the excellent oxidation resistance of the NiCoCrAlYTa coating[34]. NiCoCrAlYTa is a spraying material with high temperature oxidation resistance, which can be used at temperatures up to 1050 ℃. It can be seen from Fig. 2 that the shape of the powder particles is mainly spherical, and some smaller spherical objects are attached to the surface of the particles. The cast dendrite structure also exists on the surface of spherical particles. The reason for the appearance of as-cast dendrites may be that the growth direction of the grains is opposite to the direction of heat dissipation. Since the heat is dissipated from the inside to the outside, the grains grow from the outside to the inside, thus growing into dendrites, but in the center of the liquid alloy , the heat is dissipated to the surroundings, so the grains in the center grow to the surroundings. In addition, the diffusion rate of alloying elements cannot keep up with the cooling rate, so a local cast dendrite structure is produced.

Table 3. Chemical composition of NiCoCrAlYTa powder (wt.%).

Ni	Co	Cr	Al	Ta	Y	Other
Bal.	20-26	18-23	6-11	2-6	0.3-0.9	N.R.

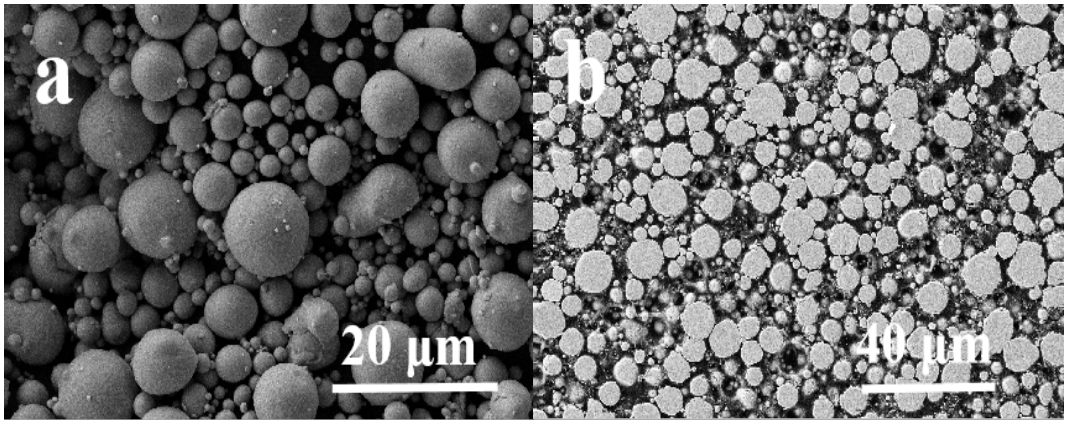

Fig. 2. (a) Morphologies of NiCoCrAlYTa powder; (b) Cross-section of NiCoCrAlYTa powder.

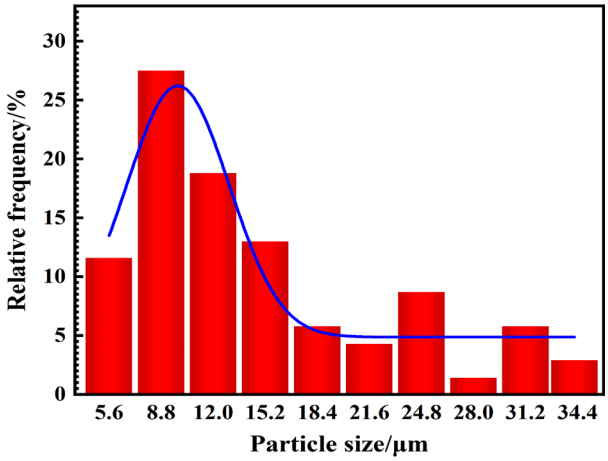

Fig. 3. Particle size distribution of NiCoCrAlYTa powder.

The TG-DTA curve of NiCoCrAlYTa powder is shown in Fig. 4. Among them, the melting points of nickel, cobalt, chromium, aluminum, yttrium and tantalum are 1455 ℃, 1495 ℃, 1857 ℃, 660 ℃, 1522 ℃ and 2996 ℃, respectively. It is clear from the nature of these material elements that the increase in powder weight is due to the oxidation reaction of nickel with aluminum. Among them, the slow increase in weight from 200 ℃ to 808 ℃ is because elements such as nickel and aluminum form a primary oxide protective film, which can prevent the powder body from being further oxidized. Corresponding to the exothermic peak that appears around 500 ℃. The rapid increase in weight after 808 ℃ is due to the increased oxidation reaction of the powder. It can be seen that the NiCoCrAlYTa powder is very stable under 808 ℃.

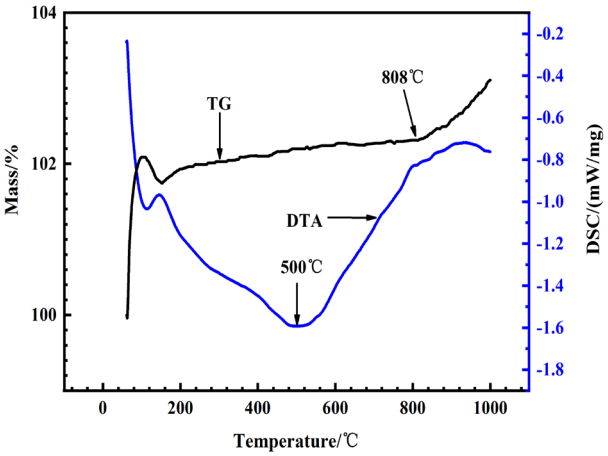

Fig. 4. TG-DTA curve of NiCoCrAlYTa.

Table 4 shows the chemical composition of 8YSZ powder. The 8YSZ powder preparation process is agglomeration and plasma densification. 8YSZ powders were agglomerated by spray drying and then treated with high temperature and low velocity nitrogen/hydrogen plasma, which

would allow the particles to remain at high temperature for sufficient time to fuse to form a homogeneous hollow structure with a solid outer shell[35]. The thickness of the solid shell is about 2%-20% of the powder particle diameter. As a result, the plasma densified hollow spherical powder has a very smooth surface, improved flowability and high cost. As shown in Fig. 5, most of the 8YSZ powders are regular spherical with dense surface. The powder has excellent flowability. Part of the powder is broken. The internal structure can be seen from the cross-section of the broken powder, most of which are hollow spherical powders with dense outer shell and porous inner powder. The particle size distribution of 8YSZ powder is shown in Fig. 6. The hollow spherical powder is formed by the agglomeration of fine particles with a size of about 500 nm. According to the EDS surface scan elemental analysis as in Fig. 5(d), it can be concluded that the main elements of the powder are Zr, O and Y. The composition of the powder is uniform.

Table 4. Chemical composition of 8YSZ powder (wt.%).

ZrO_2	Y_2O_3	SiO_2	TiO_2	Al_2O_3	Fe_2O_3	Other oxides	Monoclinic phase
Bal.	8.0	0.3	0.2	0.2	0.2	1.0	10

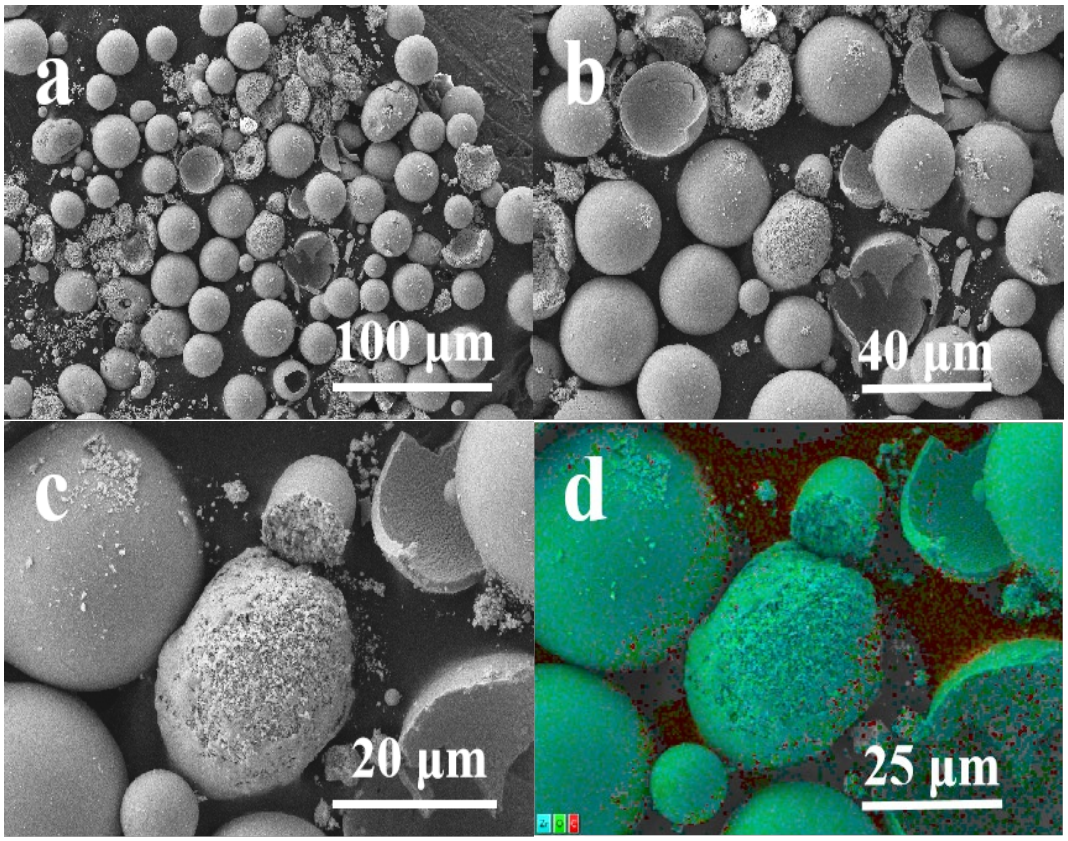

Fig. 5. (a), (b) and (c) Microstructure of 8YSZ powder; (d) EDS analysis.

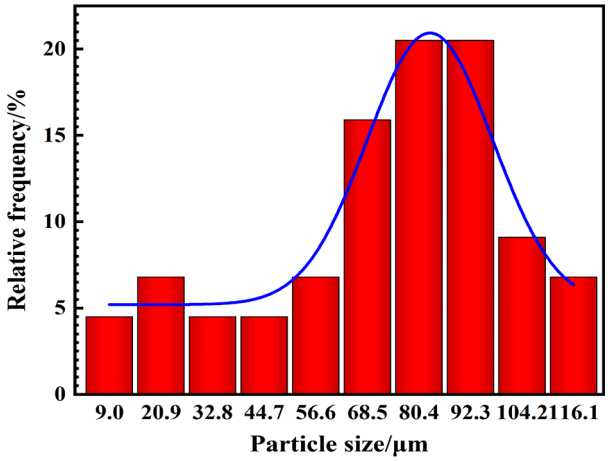

Fig. 6. Particle size distribution of 8YSZ powder.

The cross-section of 8YSZ powder is shown in Fig. 7. It can be seen that the cross-sectional shape of the powder is a regular circle, and the powder contains some fine particles, showing an obvious hollow spherical powder. This is related to the preparation process of the powder. Figure 8 shows the TG-DTA curve of 8YSZ powder in air. Zirconia transforms from monoclinic phase to tetragonal phase at 1173 ℃, and is basically stable below 1000 ℃.

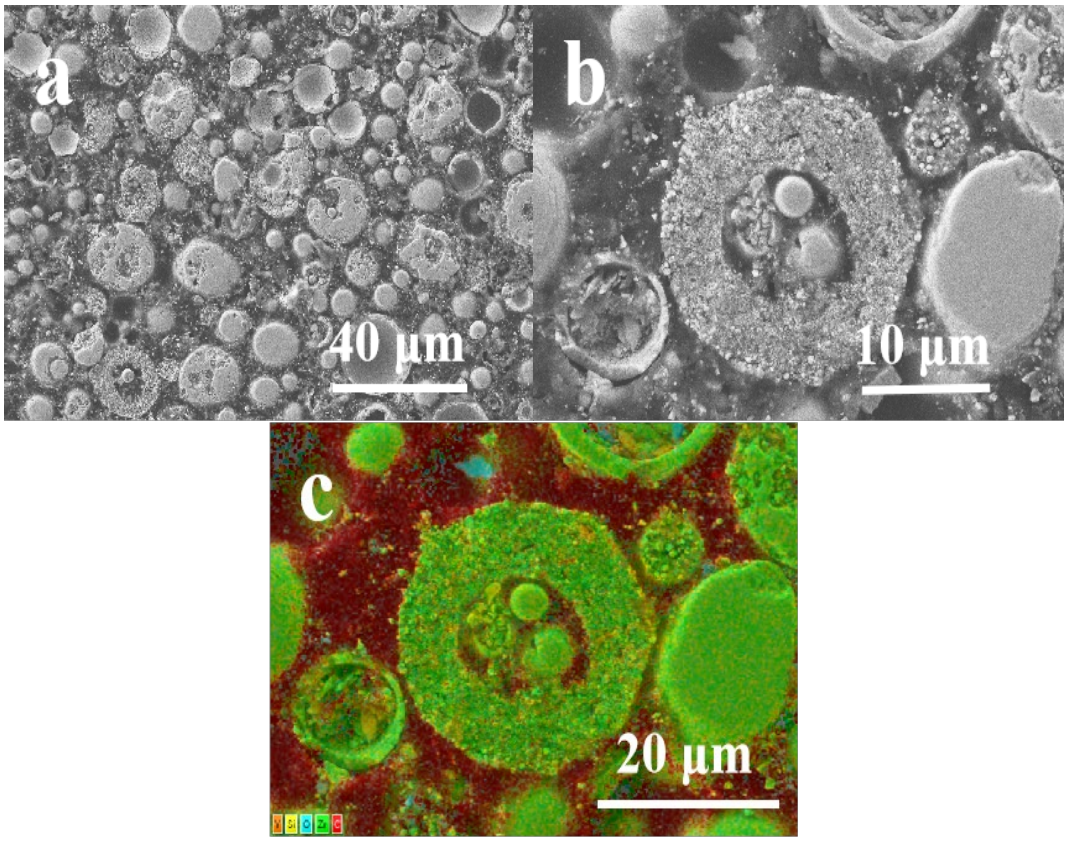

Fig. 7. (a) and (b) 8YSZ powder cross-section; (c) EDS analysis.

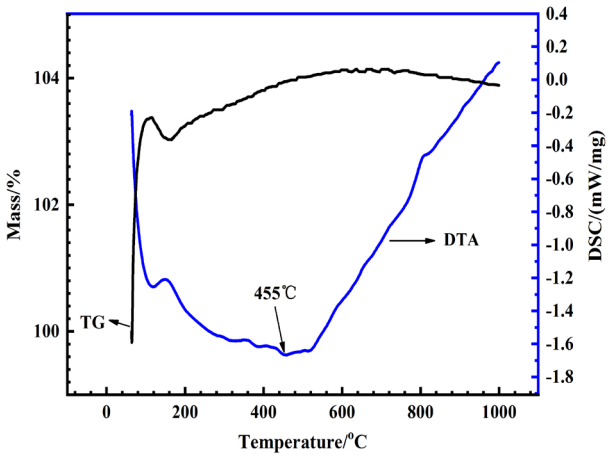

Fig. 8. TG-DTA curve of 8YSZ powder.

3.2. Coating characteristics

Fig. 9 shows the surface morphology of the NiCoCrAlYTa coating, the surface of the sprayed coating is usually very rough. There are some semi-melted and unfelted particle areas.The relatively flat areas visible on the surface of the NiCoCrAlYTa coating are caused by the high speed of the droplets hitting the coating during the spraying process. And it can be observed that the coating prepared by atmospheric plasma spraying technique has a typical porous layered structure as shown in Fig. 10. The NiCoCrAlYTa coating consists of a dark gray β-NiAl phase and a light gray γ-Ni phase[36]. It has been shown[37]that the thermal barrier coating life was more than doubled by using MCrAlY alloy as a bond coating.

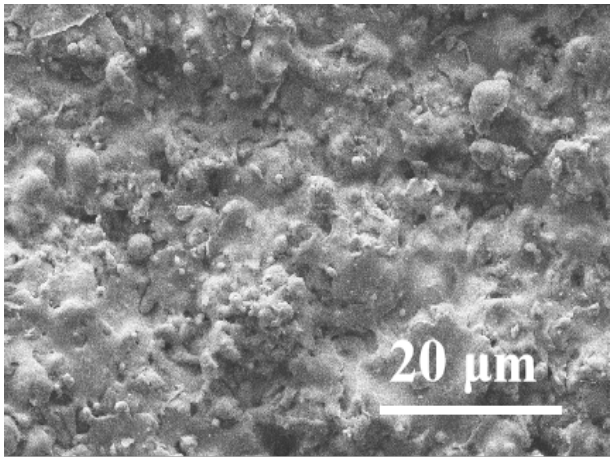

Fig. 9. Surface morphology of NiCoCrAlYTa coating.

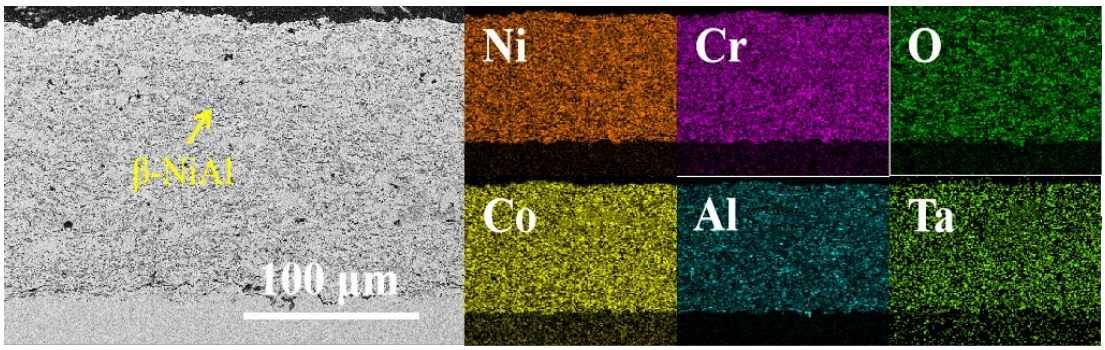

Fig. 10. Cross-sectional image and element mapping of NiCoCrAlYTa coating.

Fig. 11 shows the surface morphology of the 8YSZ thermal barrier coating. In terms of morphology, the coating surface is uneven, the organization is not uniform and dense enough, and the distribution of microscopic cracks can be observed. The coating consists of layered flakes with clearly visible pores between the layers. The cracks on the surface of the coating are mainly attributed to the brittleness of the ceramic coating and the large tensile stress generated by the condensation and shrinkage of the ceramic droplets. Fig. 12 shows the cross-sectional structure of the plasma sprayed TBC. The composition of the TBC can be clearly seen in the figure: ceramic layer (8YSZ), metal bonded coating (NiCoCrAlYTa) and substrate. As the surface of the substrate is roughened by sandblasting, it is microscopically uneven, which makes a good "hook and bite" between the substrate and the bond coating and helps to improve the bonding strength of the coating and the substrate. The results show that there is a clear demarcation line existing between both the substrate and the bond coating, and between the bond coating and the ceramic coating, all of which are dominated by mechanical bonding.

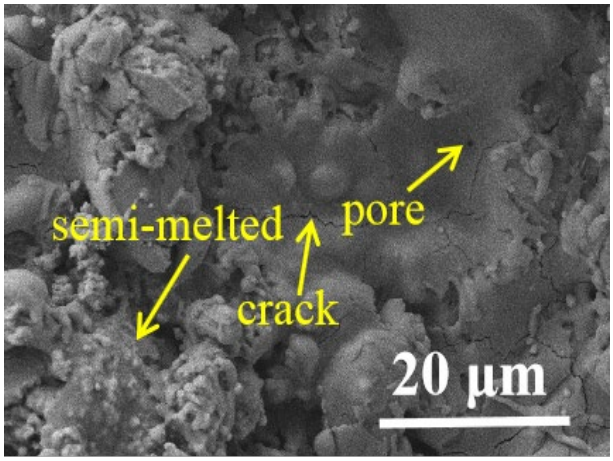

Fig. 11. Surface morphology of 8YSZ coating.

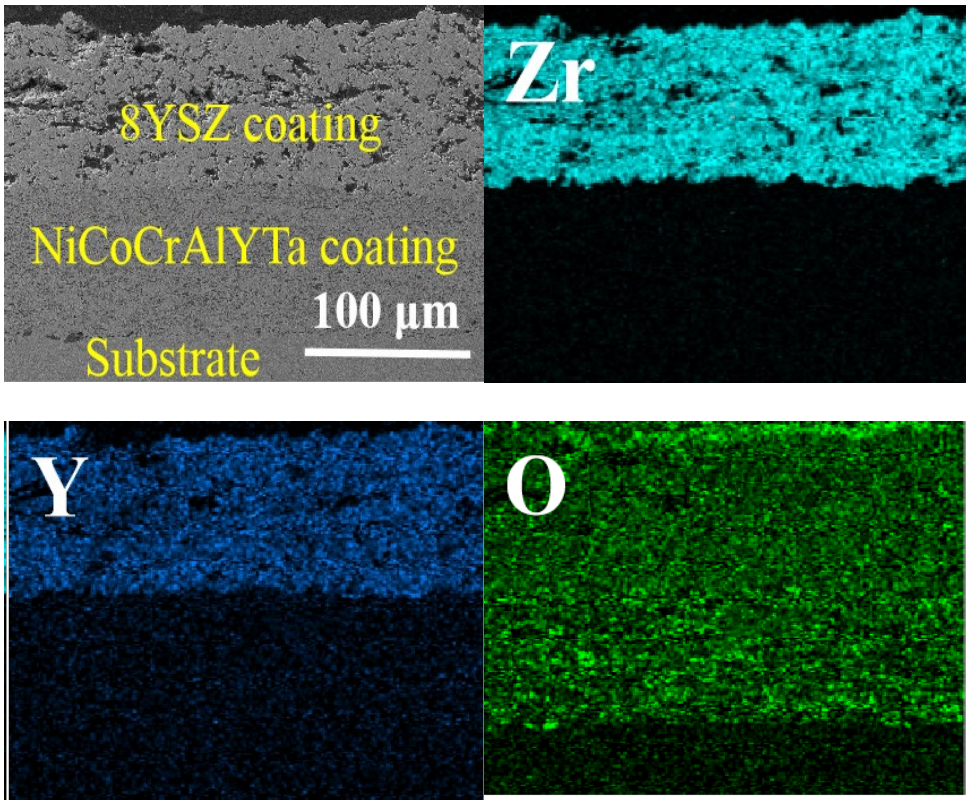

Fig. 12. Cross-sectional image and element mapping of 8YSZ coating.

Fig. 13 shows the XRD patterns of 8YSZ powder and coating, 8YSZ powder consists of tetragonal phase (t'-ZrO_2). Only a single tetragonal phase (t'-ZrO_2) exists in the 8YSZ coating. No other monoclinic or cubic zirconia related peaks exist. The combination of yttria and zirconia stabilizes the structure in a stable tetragonal phase (t'-ZrO_2).

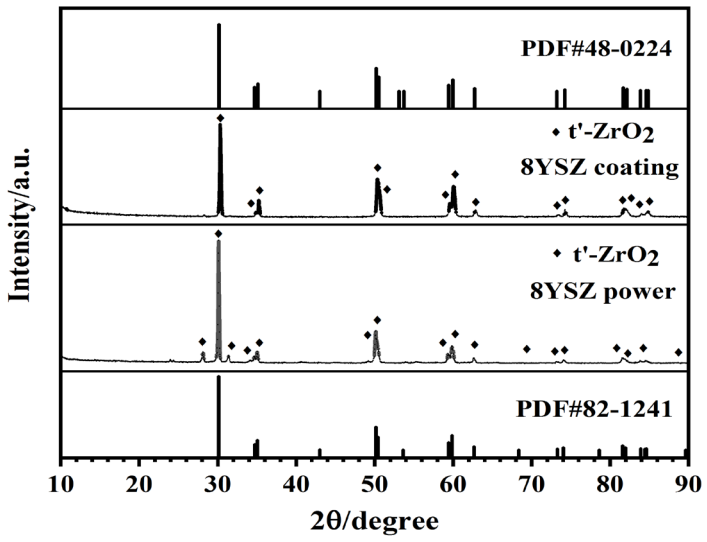

Fig. 13. XRD pattern of 8YSZ powder and coating.

The hardness of the coating is a very important mechanical performance index, which is closely related to the wear resistance, strength and service life of the coating. When measuring, it is necessary to avoid defect positions such as oxides and pores as much as possible. The measured values of the six points are shown in Table 5. The average Vickers hardness of 8YSZ coating is 595 $HV_{0.3}$. In addition, there is a large fluctuation in the measured hardness values due to defects such as coating porosity and the denseness of the microstructure having a large effect on the coating microhardness[38]. Fig. 14 shows confocal microscopic images of the surface of the 8YSZ coating, which has a surface roughness of 6.4 μm. Taking the effective fracture of the tensile sample, the bonding strength of the sample coating is measured to be 36 MPa, 37 MPa and 39 MPa respectively, and the average bonding strength of the coating is 37 MPa. It meets the requirements of the working requirements of gas turbines that the bonding strength is ≥35 MPa.

Table 5. Vickers hardness of 8YSZ coating.

Number	1	2	3	4	5	6
Hardness value	595	558	510	680	737	492
Average value	595					

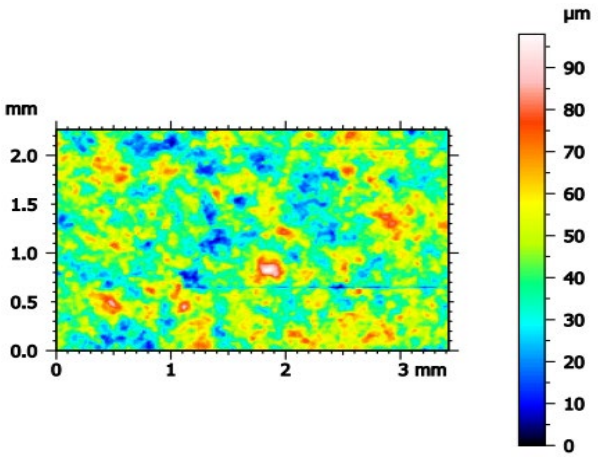

Fig. 14. Confocal microscope image of 8YSZ coating.

The macroscopic surface morphologies of the 8YSZ thermal barrier coated aluminum alloy piston after different thermal cycles are prepared as shown in Fig. 15. After 70 thermal cycles, the surface of the aluminum alloy piston did not change significantly and the coating did not break or peel off, which proves that the prepared piston thermal barrier coating can withstand the severe working environment at 550 ℃. Fig. 16 is a trend diagram of the overall mass change of the aluminum alloy piston during the thermal cycle experiment. It can be seen that the mass change of the aluminum alloy piston before and after the thermal cycle test is relatively stable, and the change range is small.

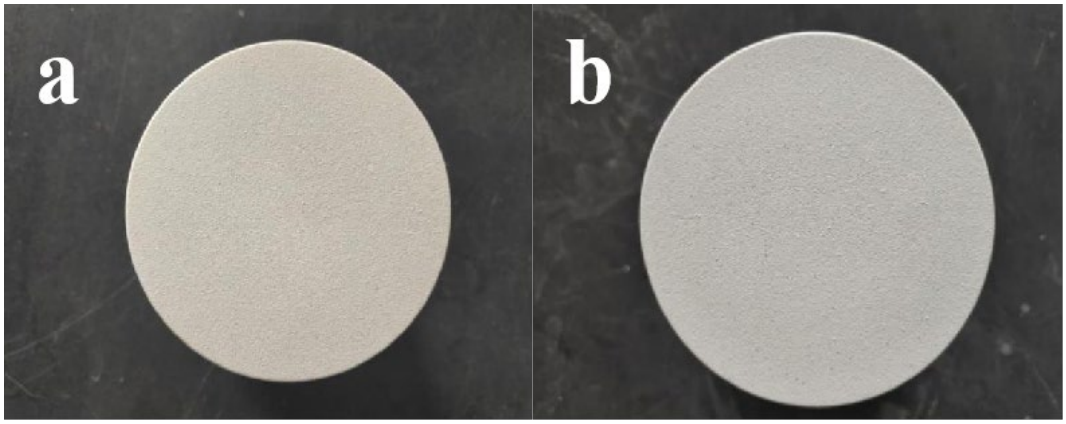

Fig. 15. Macroscopic surface morphology of aluminum piston 8YSZ thermal barrier coating after different thermal cycles: (a) 0 times; (b) 70 times.

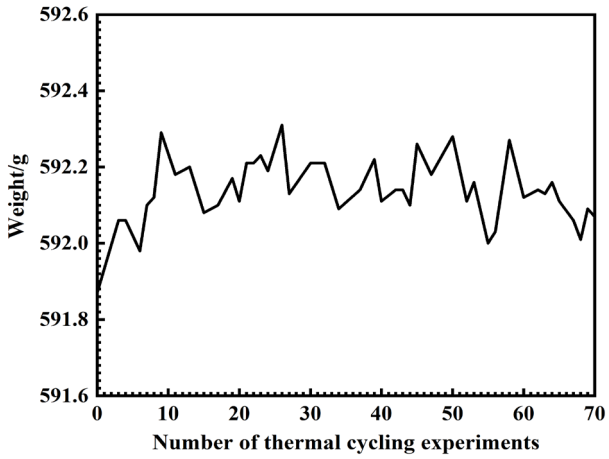

Fig. 16. Weight changes of aluminum alloy pistons in thermal cycle experiments.

The temperature field distribution cloud diagram of the aluminum alloy piston is shown in Fig 17. From Figure 17 (a), it can be seen that the temperature distribution of the aluminum alloy piston during operation gradually decreases along the Z axis, and the highest temperature is the top of the piston, which can reach 253.94 ℃, which conforms to the limit range of the highest operating temperature of the aluminum alloy piston at 370 ℃. The lowest temperature part is the piston skirt, the temperature is 93.296 ℃. The temperature field distribution of the piston after preparing the 8YSZ coating is shown in Figure 17 (b). The temperature of the top of the aluminum alloy piston reached 276.12 ℃, which was about 22 ℃ higher than that of the piston without thermal barrier coating. The depth of the high-temperature distribution area of the aluminum alloy piston with the thermal barrier coating was abruptly reduced compared with that of the piston without the thermal barrier coating, proving that the thermal barrier coating not only serves to isolate heat, but also protects the aluminum alloy substrate from damage caused by high temperatures and improves service life.

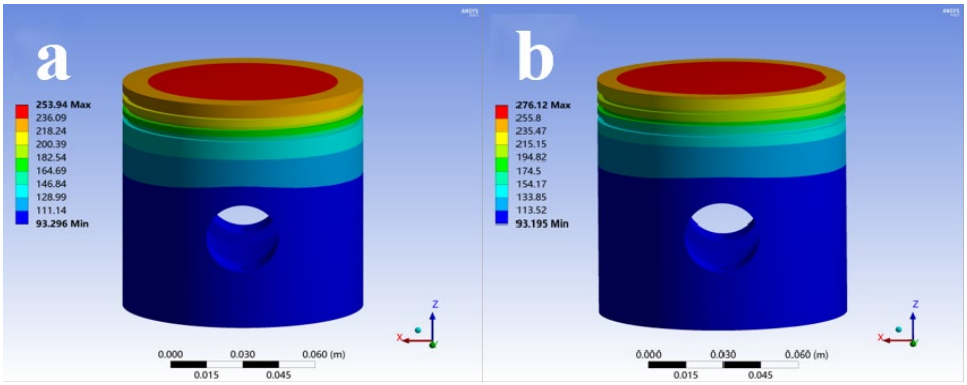

Fig. 17. Cloud diagram of temperature field distribution of aluminum alloy piston: (a) without coating; (b) with coating.

Fig. 18 shows the potentiodynamic polarization curves of YSZ coating and substrate in 3.5 wt% NaCl solution, and the fitted data obtained by Tafel extrapolation method are shown in Table 6. The corrosion potential (E_{corr}) reflects the corrosion tendency of the coating, the more positive the Ecorr, the smaller the corrosion tendency. The corrosion current density (i_{corr}) is proportional to the corrosion rate[39], the lower the i_{corr}, the better the corrosion resistance[40, 41]. The E_{corr} of 8YSZ coating and substrate are -0.26, -0.77 V, corrosion current density is 1.78×10^{-7}, 1.09×10^{-5} A·cm^{-2}, respectively. The E_{corr} of 8YSZ coating is more positive, and the i_{corr} of 8YSZ coating is smaller than that of substrate, which indicates that the coating has better corrosion resistance. Fig. 19 shows the Nyquist plots of 8YSZ coating and substrate immersed in 3.5 wt% NaCl solution. In this study, the Nyquist plots of the coatings also exhibit different corrosion behaviors. The diameter of the capacitive circuit formed in the Nyquist plot plays a very important role in the evaluation of the corrosion resistance of the coating. The larger the diameter of the capacitive circuit, the more resistant it is to corrosive media[42]. Compared with the substrate, 8YSZ coating has better corrosion resistance.

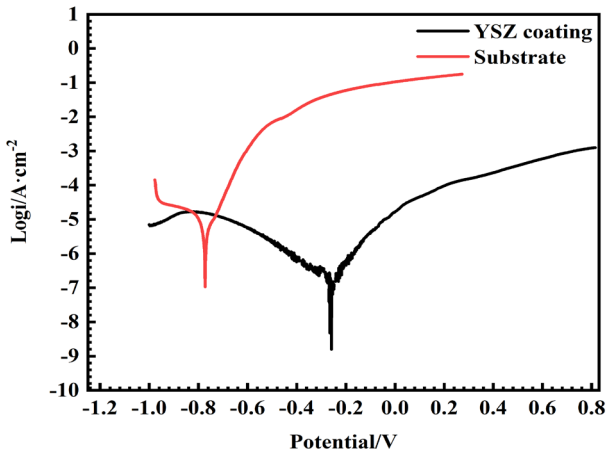

Fig. 18. Potentiodynamic polarization curves of 8YSZ coating and substrate.

Table 6. Fitting results of polarization curves.

Samples	β_a(V·dec^{-1})	$-\beta_c$(V·dec^{-1})	E_{corr}(V)	I_{corr}(A·cm^{-2})
Substrate	16.57	2.25	−0.77	1.09×10^{-5}
8YSZ coating	8.55	4.09	−0.26	1.78×10^{-7}

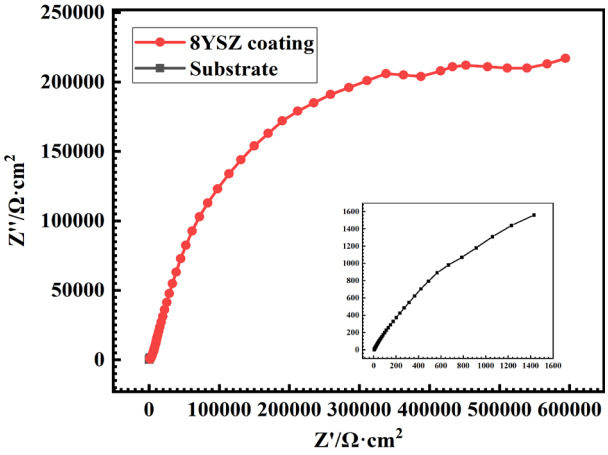

Fig. 19. Nyquist plots of 8YSZ coating and substrate.

4. Conclusion

In this study, 8YSZ TBCs were successfully prepared by atmospheric plasma spraying technology. The TBCs use NiCoCrAlYTa bond coating, which is beneficial to prolong the life of the TBCs. The overall shape of 8YSZ coating is smooth and has a stable tetragonal phase. 8YSZ coating has a bond strength of 37 MPa, Vickers hardness of 595 $HV_{0.3}$ and surface roughness of 6.4 μm, which meets the requirements of the workpiece. The 8YSZ coating has good thermal shock resistance and remains intact after 70 thermal cycle experiments. The finite element results show that the surface temperature of the piston sprayed with thermal barrier coating increases and the temperature of the piston body decreases, and the 8YSZ coating can insulate heat. The electrochemical experimental results show that the 8YSZ coating has good corrosion resistance.

Acknowledgements

The project was supported by Qilu University of Technology (Shandong Academy of Sciences) - Weihai City Industry-University-Research Collaborative Innovation Fund 2022CXY-03.

References

[1] A. Ghaseminezhad Koushali, M. Sameezadeh, M. Vaseghi and P. Safarpour, Surface and Coatings Technology **337**, 90 (2018); http://doi.org/10.1016/j.surfcoat.2018.01.010
[2] M. Bäker and P. Seiler, Journal of Thermal Spray Technology **26**(6), 1146 (2017); http://doi.org/10.1007/s11666-017-0592-z
[3] W. G. Mao, Y. Y. Chen, Y. J. Wang, M. Zhou, H. Y. Yang, Z. Wang, C. Y. Dai, X. Chen and D. N. Fang, Surface and Coatings Technology **350**, 211 (2018); http://doi.org/10.1016/j.surfcoat.2018.07.013
[4] K. Ma and J. M. Schoenung, Philosophical Magazine Letters **90**(10), 739 (2010); http://doi.org/10.1080/09500839.2010.506424
[5] T. A. Taylor and P. N. Walsh, Surface and Coatings Technology **177-178**, 24 (2004); http://doi.org/10.1016/j.surfcoat.2003.05.001
[6] Z. X. Yu, J. B. Huang, W. Z. Wang, J. Y. Yu and L. M. Wu, Surface and Coatings Technology **288**, 126 (2016); http://doi.org/10.1016/j.surfcoat.2016.01.001
[7] X. Chen, Y. Sun, D. Chen, J. Li, W. Li, D. Zeng, D. Wu, B. Zou and X. Cao, Journal of the European Ceramic Society **39**(13), 3778 (2019); http://doi.org/10.1016/j.jeurceramsoc.2019.04.055
[8] G. Lyu, B.-G. Choi, Z. Lu, H.-M. Park, Y.-G. Jung and J. Zhang, Surface and Coatings Technology **364**, 187 (2019); http://doi.org/10.1016/j.surfcoat.2019.02.069
[9] A. Kulkarni, A. Vaidya, A. Goland, S. Sampath and H. Herman, Materials Science and Engineering A **A359**(1-2), 100 (2003); http://doi.org/10.1016/s0921-5093(03)00342-3
[10] C. G. Levi, Current Opinion in Solid State and Materials Science **8**(1), 77 (2004); http://doi.org/10.1016/j.cossms.2004.03.009
[11] J. Huang, W. Wang, J. Yu, L. Wu and Z. Feng, Journal of Thermal Spray Technology **26**(4), 755 (2017); http://doi.org/10.1007/s11666-017-0547-4
[12] F. Guo, C. Xing, G. Wang, Z. Zou, X. Wang, Q. Zhang, X. Zhao and P. Xiao, Materials & Design **139**, 343 (2018); http://doi.org/10.1016/j.matdes.2017.11.022
[13] Z. X. Yu, W. Z. Wang and H. H. Wang, Journal of Thermal Spray Technology **23**(8), 1436 (2014); http://doi.org/10.1007/s11666-014-0147-5
[14] U. Schulz, B. Saruhan, K. Fritscher and C. Leyens, International Journal of Applied Ceramic Technology **1**(4), 302 (2004); http://doi.org/10.1111/j.1744-7402.2004.tb00182.x
[15] S. Rezanka, G. Mauer and R. Vaßen, Journal of Thermal Spray Technology **23**(1-2), 182 (2013); http://doi.org/10.1007/s11666-013-9971-2
[16] A.G.Evans, D.R.Mumm, J.W.Hutchinson, G.H.Meier and F.S.Pettit, Progress of Materials Science **46**, 505 (2001); http://doi.org/10.1016/s0079-6425(00)00020-7
[17] X. Q. Cao, R. Vassen and D. Stoever, Journal of the European Ceramic Society **24**(1), 1 (2004); http://doi.org/10.1016/s0955-2219(03)00129-8
[18] B. Li, X. Fan, T. Wang and K. Zhou, Engineering Fracture Mechanics **201**, 13 (2018); http://doi.org/10.1016/j.engfracmech.2018.08.026
[19] Z. Zou, C. Xing, L. He, X. Shan, L. Luo, X. Zhao, F. Guo and P. Xiao, Journal of the American Ceramic Society **101**(9), 4375 (2018); http://doi.org/10.1111/jace.15697
[20] Z. Zhao, H. Chen, H. Xiang, F.-Z. Dai, X. Wang, W. Xu, K. Sun, Z. Peng and Y. Zhou, Journal of Advanced Ceramics **9**(3), 303 (2020); http://doi.org/10.1007/s40145-020-0368-7

[21] R. A. Miller, Journal of Thermal Spray Technology **6**,35 (1997); http://doi.org/10.1007/bf02646310_
[22] M. J. Pomeroy, Materials & Design **26**(3), 223 (2005); http://doi.org/10.1016/j.matdes.2004.02.005
[23] J. Jiang, W. Wang, X. Zhao, Y. Liu, Z. Cao and P. Xiao, Engineering Fracture Mechanics **196**, 191 (2018); http://doi.org/10.1016/j.engfracmech.2018.04.031
[24] J. Jiang, L. Jiang, Z. Cai, W. Wang, X. Zhao, Y. Liu and Z. Cao, Surface and Coatings Technology **357**, 433 (2019); http://doi.org/10.1016/j.surfcoat.2018.10.020
[25] L. Wang, Z. Tan, S. Wang, W. Liu, J. Hao, X. Zhang, S. Deng, C. Yu, H. Zheng, Z. Zeng, H. Lu, L. He and J. Chen, Journal of Materials Processing Technology **316**, 117966 (2023); http://doi.org/10.1016/j.jmatprotec.2023.117966
[26] S. Salam, P. Y. Hou, Y. D. Zhang, H. F. Wang, C. Zhang and Z. G. Yang, Corrosion Science **95**, 143 (2015); http://doi.org/10.1016/j.corsci.2015.03.011
[27] N. Vermaak, A. Mottura and T. M. Pollock, Corrosion Science **75**, 300 (2013); http://doi.org/10.1016/j.corsci.2013.06.013
[28] X. Gong, R. R. Chen, Y. H. Yang, Y. Wang, H. S. Ding, J. J. Guo, Y. Q. Su and H. Z. Fu, Applied Surface Science **431**, 81 (2018); http://doi.org/10.1016/j.apsusc.2017.07.026
[29] Y. Han, Z. Zhu, B. Zhang, Y. Chu, Y. Zhang and J. Fan, Journal of Alloys and Compounds **735**, 547 (2018); http://doi.org/10.1016/j.jallcom.2017.11.165
[30] A. K. Ray, N. Roy, A. Kar, A. K. Ray, S. C. Bose, G. Das, J. K. Sahu, D. K. Das, B. Venkataraman and S. V. Joshi, Materials Science and Engineering: A **505**(1-2), 96 (2009); http://doi.org/10.1016/j.msea.2008.11.066
[31] S. Stecura, Thin Solid Films **73**, 481 (1980); http://doi.org/10.1016/0040-6090（80）90521-0
[32] P. Choquet and R. Mevrel, Materials Science and Engineering: A **120**, 153 (1989); http://doi.org/10.1016/0921-5093(89)90733-8
[33] R. Chen, X. Gong, Y. Wang, G. Qin, N. Zhang, Y. Su, H. Ding, J. Guo and H. Fu, Corrosion Science **136**, 244 (2018); http://doi.org/10.1016/j.corsci.2018.03.008
[34] D. Zhang, J. Liu, Z. Xue and X. Mao, Surface and Coatings Technology **252**, 179 (2014); http://doi.org/10.1016/j.surfcoat.2014.04.064
[35] S. Zhou, S. Shen, Y. Chen, Z. Zhang and S. Wu, Materials Chemistry and Physics **259**, 124018 (2021); http://doi.org/10.1016/j.matchemphys.2020.124018
[36] W. X. Weng, Y. M. Wang, Y. M. Liao, C. C. Li and Q. Li, Surface and Coatings Technology **352**, 285 (2018); http://doi.org/10.1016/j.surfcoat.2018.08.024
[37] J. He, Surface and Coatings Technology **448**,128931 (2022); http://doi.org/10.1016/j.surfcoat.2022.128931
[38] H. Qazi Lavasani, Z. Valefi, N. Ehsani and S. Tamaddon Masoule, Ceramics International **43**(15), 12497 (2017); http://doi.org/10.1016/j.ceramint.2017.06.120
[39] A. A. Rodriguez, J. H. Tylczak, M. C. Gao, P. D. Jablonski, M. Detrois, M. Ziomek-Moroz and J. A. Hawk, Advances in Materials Science and Engineering **2018**, 1 (2018); http://doi.org/10.1155/2018/3016304
[40] D. Jiang, H. Z. Cui, H. Chen, X. F. Zhao, G. L. Ma and X. J. Song, Materials & Design **210**, 110068 (2021); http://doi.org/10.1016/j.matdes.2021.110068
[41] K. Rahmani, G. H. Majzoobi, H. Bakhtiari and A. Sadooghi, Materials Chemistry and Physics **271**, 124946 (2021); http://doi.org/10.1016/j.matchemphys.2021.124946

[42] S. K. Nayak, M. A. Faridi, G. M, A. Kumar and T. Laha, Materials Characterization **191**, 112149 (2022); http://doi.org/10.1016/j.matchar.2022.112149